Fabrication of quantum emitters in aluminum nitride by Al-ion implantation and thermal annealing

E. Nieto Hernández ⓘ ; H. B. Yağcı ⓘ ; V. Pugliese ⓘ ; P. Aprà ⓘ ; J. K. Cannon ⓘ ; S. G. Bishop ⓘ ;
J. Hadden ⓘ ; S. Ditalia Tchernij ⓘ ; P. Olivero ⓘ ; A. J. Bennett ⓘ ; J. Forneris ✉ ⓘ
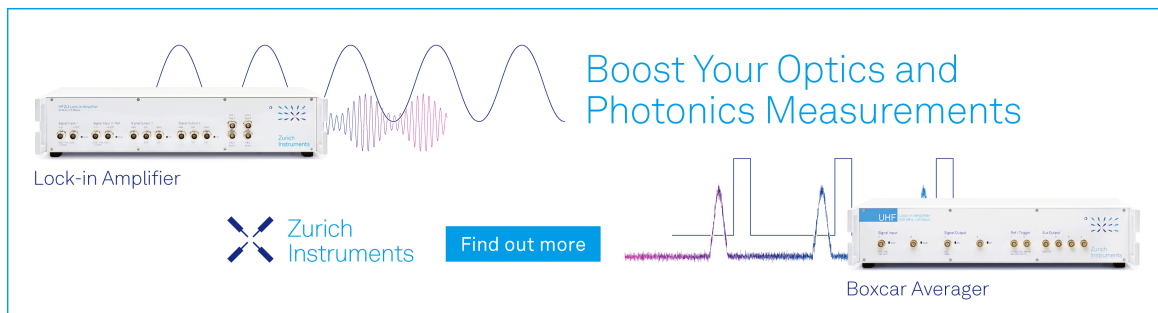
View Online   Export Citation

Fabrication of quantum emitters in aluminum nitride by Al-ion implantation and thermal annealing

View Online   Export Citation   CrossMark

E. Nieto Hernández,[1,2] (iD) H. B. Yağcı,[3,4] (iD) V. Pugliese,[1,2] (iD) P. Aprà,[1,2] (iD) J. K. Cannon,[3,4] (iD) S. G. Bishop,[3,4] (iD)
J. Hadden,[3,4] (iD) S. Ditalia Tchernij,[1,2] (iD) P. Olivero,[1,2] (iD) A. J. Bennett,[3,4] (iD) and J. Forneris[1,2,a)] (iD)

AFFILIATIONS

[1]Dipartimento di Fisica e Centro Inter-Dipartimentale "NIS," Università di Torino, via Pietro Giuria 1, Torino 10125, Italy
[2]Istituto Nazionale di Fisica Nucleare (INFN), Sezione di Torino, via Pietro Giuria 1, Torino 10125 Italy
[3]School of Engineering, Cardiff University, Queen's Building, The Parade, Cardiff CF24 3AA, United Kingdom
[4]Translational Research Hub, Cardiff University, Maindy Road, Cathays, Cardiff CF24 4HQ, United Kingdom

[a)]Author to whom correspondence should be addressed: Jacopo.forneris@unito.it

ABSTRACT

Single-photon emitters (SPEs) within wide-bandgap materials represent an appealing platform for the development of single-photon sources operating at room temperatures. Group III-nitrides have previously been shown to host efficient SPEs, which are attributed to deep energy levels within the large bandgap of the material, in a configuration that is similar to extensively investigated color centers in diamond. Anti-bunched emission from defect centers within gallium nitride and aluminum nitride (AlN) have been recently demonstrated. While such emitters are particularly interesting due to the compatibility of III-nitrides with cleanroom processes, the nature of such defects and the optimal conditions for forming them are not fully understood. Here, we investigate Al implantation on a commercial AlN epilayer through subsequent steps of thermal annealing and confocal microscopy measurements. We observe a fluence-dependent increase in the density of the emitters, resulting in the creation of ensembles at the maximum implantation fluence. Annealing at $600\,°C$ results in the optimal yield in SPEs formation at the maximum fluence, while a significant reduction in SPE density is observed at lower fluences. These findings suggest that the mechanism of vacancy formation plays a key role in the creation of the emitters and open enticing perspectives in the defect engineering of SPEs in solid state.

Single-photon emitters (SPEs) in wide-bandgap semiconductors are promising building blocks for quantum technologies, including quantum sensing, optical quantum computing, and quantum communication.[1–3] Quantum emitters within solid-state host materials have steadily gained relevance in the last two decades. Alongside single-photon emission in quantum dots,[4] the experimental demonstration of anti-bunched emission from color centers in diamond[5] led to a vibrant scientific field focused on characterization, manipulation, and fabrication of defect systems in wide-bandgap semiconductors.[6–8] With the advancements in ion implantation technology regarding deterministic single-ion doping and nanoscale placement precision,[9–12] along with the substantial progresses in material synthesis and development in terms of controlled and selective chemical vapor deposition,[13–15] it became possible to identify and develop optically active defects with

stable and efficient single-photon emission, that in several instances is correlated with their (highly coherent) spin properties. To date, a multitude of single-photon emitters in wideband-gap semiconductors have been reported, both in the visible and in the infrared spectral regions.[16–19] The two most widely investigated materials in this field are diamond[20–24] and silicon carbide (SiC).[16,25–27] Nonetheless, remarkable properties have been also demonstrated in other materials, such as silicon (Si),[28–30] gallium nitride (GaN),[17,31,32] hexagonal boron nitride (hBN),[33–35] and aluminum nitride (AlN).[36–38] Aluminum nitride (AlN) is a wide-bandgap semiconductor ($E_g = 6.03$ eV) with a refractive index of ~ 2.15 at $\lambda = 650$ nm. It is well known and employed as a piezoelectric material, a durable ceramic, and the ideal buffer layer for GaN growth,[39] making it an appealing semiconductor for the implementation of high-power electronics and next-generation

photonics. Following theoretical studies suggesting the availability of optical dopants with spin properties similar to those of the diamond-based nitrogen-vacancy center,[40–42] the experimental demonstration of single-photon emission from native AlN luminescent defects was recently reported.[30,37,38] A subsequent study also showed the possibility to create luminescent extrinsic defects related via controlled laser-induced damage to the AlN crystal interface with a sapphire substrate.[43] However, the origin of these emitters is still not fully understood.

In this work, we investigate the manufacturability of single-photon emitters in AlN thin films by means of Al ion implantation and subsequent thermal annealing in order to identify a reliable protocol to produce single-photon emitters from intrinsic point defects. We use Al ion implantation to promote the formation of lattice vacancies without introducing extrinsic defect complexes (i.e., defects related to the introduction of foreign chemical species) into the material. We investigate the correlation between the implantation fluence and the overall photoluminescence (PL) emission intensity from the implanted crystal, leaving out of the study the discrimination between the implanted quantum emitters and the previously present in the material. Furthermore, we assess the role of the subsequent thermal annealing to both activate individual luminescent centers and reduce the radiation-induced background emission. Finally, by means of confocal photoluminescence characterization, we show that vacancy-related quantum light emitters in AlN can be reliably fabricated by means of ion implantation combined with suitable thermal processing.

The experiments were performed on a 1 μm thick metal-organic chemical vapor deposition (MOCVD)-grown AlN epilayer on sapphire purchased from Dowa Electronics Materials Co. The material is a wurtzite-type single crystal and contains native optically active defects dispersed with low density.[38] The overall procedure adopted for the fabrication and characterization of the samples is highlighted in Fig. 1. In particular, Fig. 1(a) shows the fabrication process performed on the substrate. The implantation of Al ions induces the formation of lattice vacancies, whose diffusion and recombination are promoted by means of thermal annealing. The resulting effect is the formation of optically active color centers. Specifically, the sample was implanted with 60 keV Al$^-$ ions with the recently established multi-elemental ion source of the Solid State Physics laboratories of the University of Torino. Several circular regions of ø $\sim$ 1 mm were implanted at different fluences in the 10^{12}–10^{14} cm^{-2} range by means of a movable collimating mask. Figure 1(b) shows the ion implantation profile for the considered energy as a function of the sample depth along with the

corresponding vacancy density profile, suggesting that the implantation-induced color centers are formed within 100 nm from the surface. Post-implantation annealing treatments were performed using a tubular oven at 400 °C and a subsequent 30 min process at 600 °C in N$_2$ atmosphere.

The sample was characterized by means of PL confocal microscopy between the annealing treatments in order to assess the effects of ion implantation and annealing on the formation of optically active centers. The implanted regions were marked by means of high-power laser milling to enable the investigation of the same photoluminescent regions after each of the subsequent treatments performed on the sample. The PL analysis was performed using a custom fiber-coupled single-photon sensitive microscope equipped with a 100× dry objective (0.9 NA). Optical excitation was supplied by a 520 nm laser diode. In all measurements, a set of spectral filters defined a detection spectral window in the 550–650 nm range, thus ensuring the removal of the background originating from the chromium line of sapphire[44] and an abrupt cut off in the emitter spectra at the edges of this range. Second-order autocorrelation chronograms were acquired from isolated photoluminescent spots using a Hanbury–Brown & Twiss (HBT) interferometer implemented by a multimode fiber-fused 50:50 beam splitter coupled to two independent single-photon avalanche photodiodes (SPADs). The assessment of the density of created centers was performed by comparing the number of isolated spots found in the implanted regions by PL mapping,[45] with respect to a reference pristine region. Finally, spectral characterization at room temperature was performed on all the considered regions using a Princeton Instruments PIXIS spectrometer.

The effects of ion-induced radiation damage on the formation of color centers in AlN were investigated by PL confocal microscopy mapping as a function of implantation fluence and post-implantation annealing temperature. Figure 2 shows the PL maps (20 × 20 μm^2 area, 2 mW excitation power) of the unimplanted region and of the regions implanted at 1×10^{12}, 1×10^{13}, and 1×10^{14} cm^{-2} fluences after each of the above-mentioned thermal treatments. The maps acquired prior to any subsequent annealing (condition referred to as "as implanted" in the following) are presented in the top row of Figs. 2(a) and 2(d). The pristine region (first column) exhibits a low density of single emitters ($\sim$0.075 μm^{-2}), corresponding to individual bright spots ($\sim$50 kcps emission intensity) with respect to the background originating from the surrounding region ($\sim$2 kcps).

The region implanted at 1×10^{12} cm^{-2} fluence [Fig. 2(b)] did not exhibit any significant increase in the density of emitters
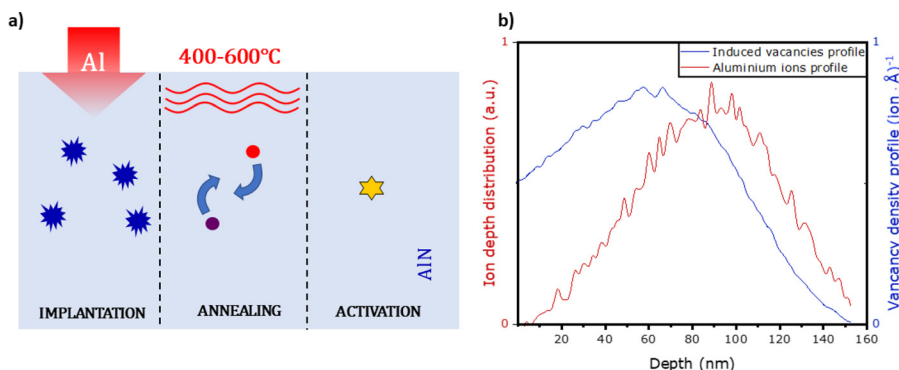
FIG. 1. Schematic overview of the experimental work. (a) Scheme of the fabrication protocol adopted in the present work. Following ion implantation, the annealing-induced thermal diffusion of vacancies and/or impurities within AlN results in the formation of stable, optically active emitters within AlN. (b) Vacancy density profile (blue) and the implanted Al ion distribution (red) associated with 60 keV Al implantation, calculated via SRIM Monte Carlo code.[43]
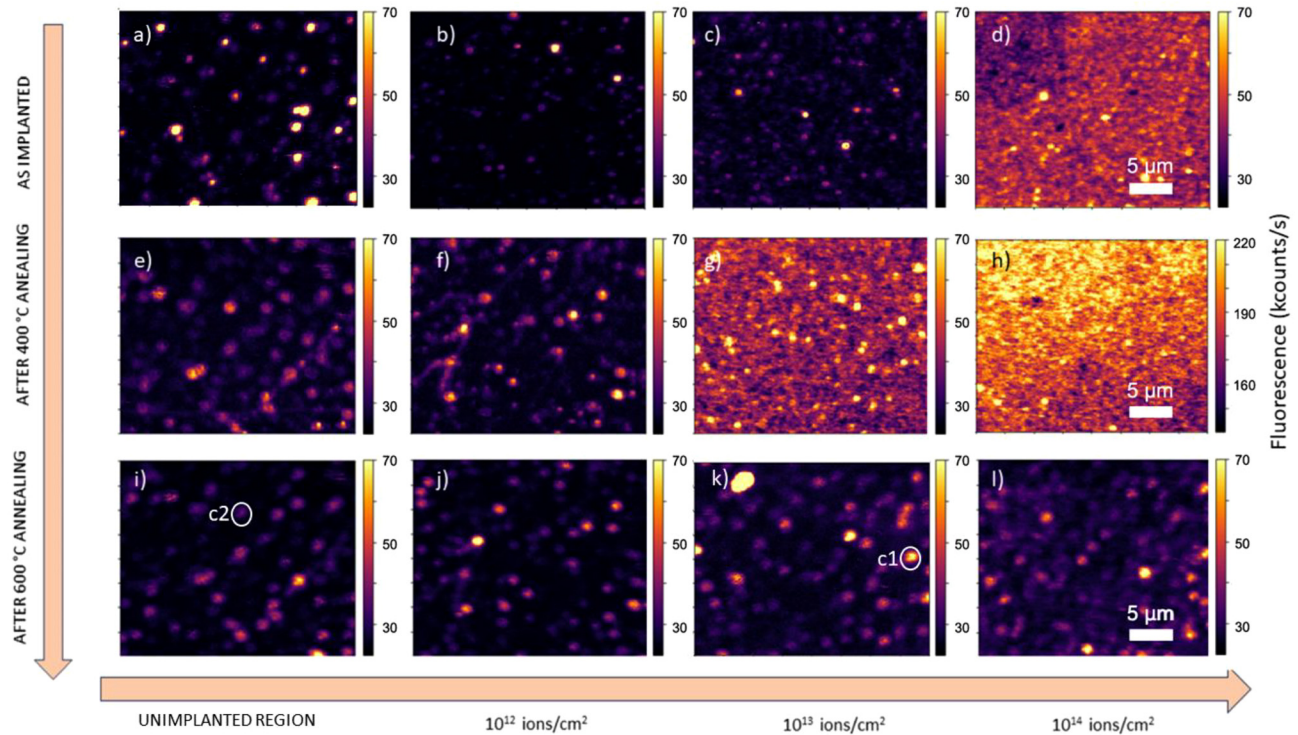
FIG. 2. PL confocal mapping of the same processed regions (20 × 20 μm^2 scan area) upon different thermal annealing steps under 520 nm laser excitation and collection window between 550 and 650 nm. The color scale encodes the range 0–70 kcps for all the considered PL scans, except for the region implanted at 1 × 10^{14} cm^{-2} fluence and annealed at 400 °C, due to the high overall emission intensity of the latter.

($\sim$0.08 μm^{-2}) with respect to the unimplanted region. In contrast, the map acquired from the region implanted at 1 × 10^{13} cm^{-2} [Fig. 2(c)] shows an increase in the emitter density ($\sim$0.37 μm^{-2}), each displaying comparable photon count rates (i.e., 60 kcps under 1 mW excitation optical power) with respect to the pristine region. This observation is indicative of the fact that the ion implantation process is responsible for the formation of optically active defects,[46] as supported by the further increase in the PL intensity ($\sim$100 kcps) observed upon ion implantation at 1 × 10^{14} cm^{-2} [Fig. 2(d)]. In the latter case, the substantial PL increase prevents the identification of individual emitters. Figures 2(d)–2(h) and Figs. 2(i)–2(l) report the PL maps (20 × 20 μm^2 area) of the unimplanted region and of the regions implanted at 1 × 10^{12}–1 × 10^{14} cm^{-2} fluences after 400 and 600 °C treatments, respectively. The same trend of the emitter density on the ion fluence, as highlighted prior to the thermal processing for all irradiation conditions, was observed. A first annealing at 400 °C did not significantly modify the emitter density in the pristine sample [Fig. 2(e)], while it resulted in an increase (0.1–0.2 μm^2) in the areal density of emitters in the regions implanted at 1 × 10^{12} [Fig. 2(f)] and 1 × 10^{13} [Fig. 2(g)] cm^{-2} fluences, although the latter was accompanied by a noticeable increase in the background PL emission. Notably, none of the native centers disappeared as a result of the 400 °C process.

The region implanted at 1 × 10^{14} cm^{-2} fluence [Fig. 2(h)] exhibited a threefold increase in the PL intensity, indicating the formation of a large density of optically active intrinsic defects, whose overall emission prevented in this case the identification of individual emitters.

The subsequent treatment at 600 °C did not alter the initial density of emitters in the pristine region [Fig. 2(i)] with respect to the previous treatments. Conversely, in the case of the second thermal process, the 1 × 10^{13}–1 × 10^{14} cm^{-2} ion fluences [Figs. 2(j)–2(l)] at the 600 °C treatment suppressed the background PL emission that was observed after the 400 °C one, thus resulting in a distribution of single emitters characterized by a higher visibility and with a 0.20–0.25 μm^{-2} areal density, respectively. In order to quantify the occurrence of single emitters following each fabrication step, the respective areal density is shown in Fig. 3 for the unimplanted sample and the regions implanted at 1 × 10^{12}–1 × 10^{14} cm^{-2}. The maximal density of emitters (0.4 μm^{-2}) is found in the 1 × 10^{13} cm^{-2} ion fluence prior to any annealing treatment. The 400 °C annealing results in a moderate increase (i.e., up to 0.2 μm^{-2}) in the emitter density for the 1 × 10^{12} cm^{-2} fluence. At higher fluences, a significant increase in the background PL is induced instead. The 600 °C annealing on the other hand results in a slight decrease in the emitter density, i.e., 0.15 μm^{-2}, which is lower than the above-mentioned corresponding value upon 400 °C processing at 1 × 10^{12} cm^{-2} ion fluence. Ultimately, the 600 °C annealing with the highest implantation fluence (1 × 10^{14} cm^{-2}) results in the formation of individual emitters. We note that for several combinations of ion fluence and annealing conditions, we are unable to quantify the density of individual emitters because of the high levels of PL coming from the whole regions, suggesting the formation of ensembles of centers not individually resolvable. These combinations have not been included in Fig. 3.
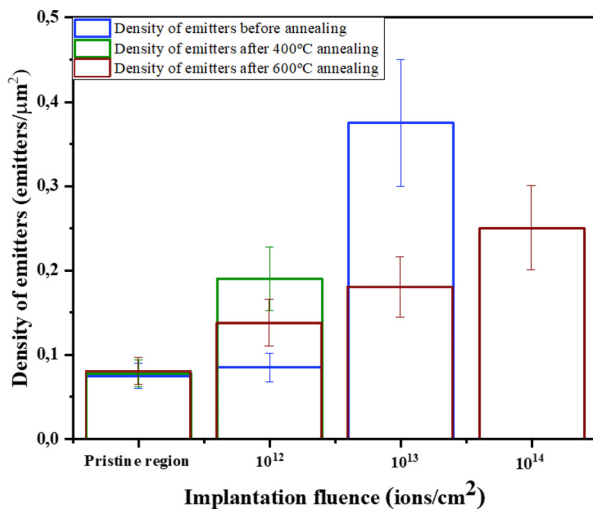
FIG. 3. Boxchart representation of the areal distribution of point-like emitters in AlN implanted at different Al–fluences following different thermal processes: untreated, 400 °C annealing, and 600 °C annealing.

The spectral features of AlN emitters were investigated systematically. A set of exemplary spectra acquired from individual emission spots is reported in Fig. 4 for different processing steps, showing the typical appearance of spectra classified as having a ZPL falling at 560 nm [Fig. 4(a), highlighted by the green marker], in the 580–600 nm range [Fig. 4(b), yellow] and at longer wavelengths [Fig. 4(c), orange], respectively.

The spectra reported in Fig. 4 are in good agreement with what has been reported in the literature, but not yet attributed to any specific defective configuration.[38] Figure 5 shows a statistical analysis of the spectral signature of a set of 58 PL spectra acquired from individual emitters. All the emitters are characterized by large (i.e., >20 nm) spectral bands. In Fig. 5(a), the ZPL wavelength distribution is shown as a function of the annealing temperature, independently of the ion implantation fluence. Conversely, Fig. 5(b) highlights the wavelength occurrence as a function of the implantation fluence, independently of the post-implantation temperature treatment. In this latter case, no centers from the region implanted at 1×10^{13} and 1×10^{14} cm^{-2} and subsequently annealed at 400 °C could be identified due to the intense background PL. In all cases, the ZPL displayed a large variability in the 560–620 nm range, with the majority of the centers emitting between 560 and 600 nm.
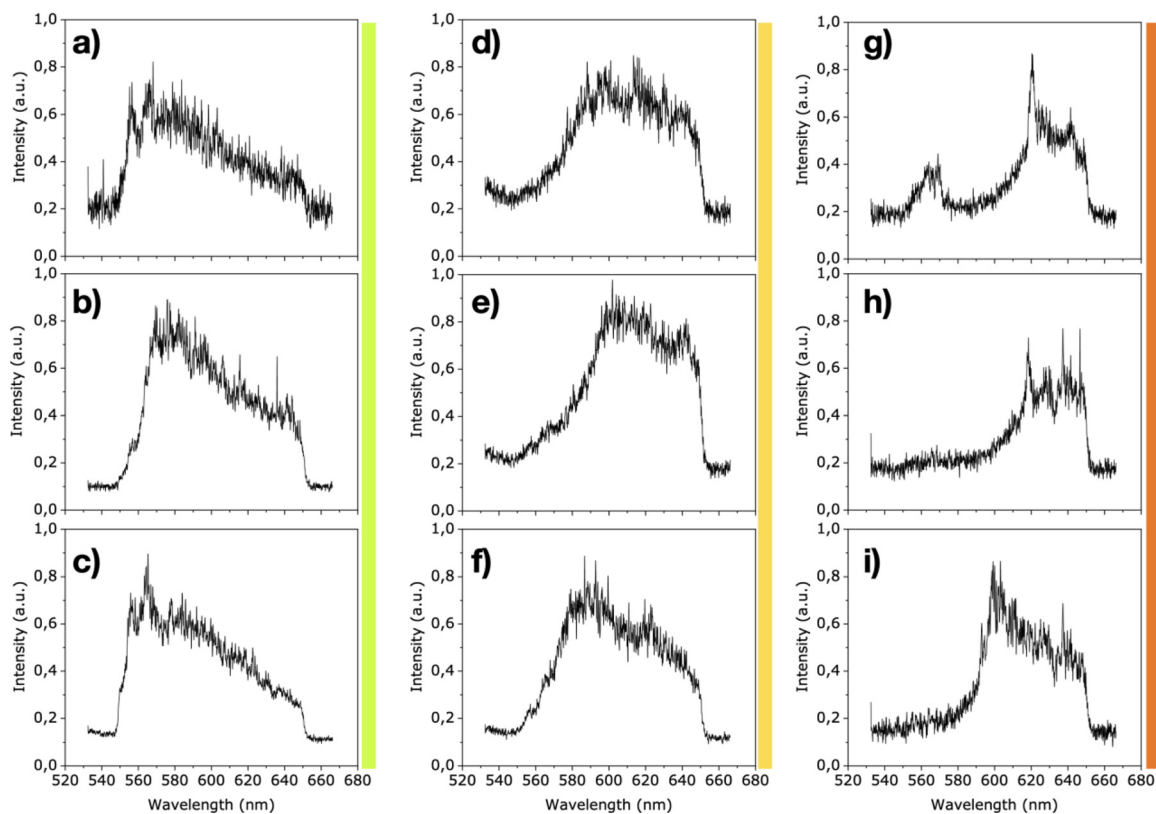
FIG. 4. Exemplary emission spectra from individual diffraction-limited spots acquired from the sample following different processing steps: (a) unimplanted sample; (b) 10^{12} cm^{-2} ion fluence, as implanted; (c) 10^{13} cm^{-2} ion fluence, 600 °C annealing; (d) unimplanted sample, 400 °C annealing; (e) 10^{12} cm^{-2} ion fluence, 400 °C annealing; (f) 10^{13} cm^{-2} ion fluence, 600 °C annealing; (g) unimplanted sample; (h) 10^{13} cm^{-2} ion fluence, as implanted; and (i) 10^{12} cm^{-2} ion fluence, as implanted.

FIG. 5. Statistical distribution of the central wavelength of the main PL emission peaks from a set of individual emitters in 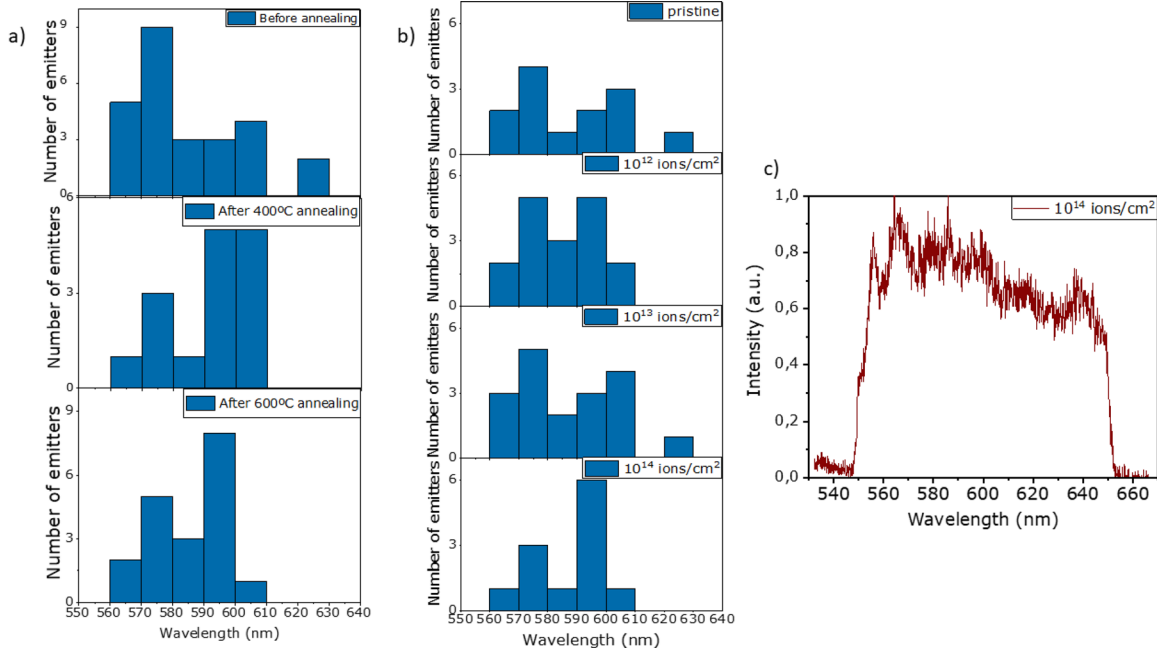AlN. (a) Distribution of the emitters at different annealing temperatures, (b) distribution for different ion implantation fluences, and (c) PL spectra of the background PL emission acquired from the region implanted at the highest ion fluence (1×10^{14} cm^{-2}) and annealed at 400 °C, corresponding to the PL map in Fig. 2(h).

The overall ZPL distribution shown in Fig. 5 suggests the occurrence of two groups of emission lines at ∼560 and ∼600 nm, which might be indicative of the presence of two different classes of emitters, or alternatively of local lattice effects on the electronic states of the point defects. This latter interpretation could be justified by the piezoelectric properties of AlN, as well as by local strains at the interface between the 1 µm thick AlN layer and the underlying sapphire substrate. To provide further context, Fig. 5(c) shows the ensemble emission spectrum acquired from the region implanted at 1×10^{14} cm^{-2} ion fluence and processed by 400 °C annealing. In this case, corresponding to the PL map shown in Fig. 2(h), the broad PL emission in the 560–640 nm range is reminiscent of the individual PL peaks observed at the single-photon emitter level, suggesting that the ensemble emission is a convolution of the multiple spectral components recorded in Figs. 4, 5(a), and 5(b). This result confirms the role of ion implantation in the formation of optically active intrinsic defects in AlN. The observation of ensemble emission with increasing intensity at the highest considered ion fluences further corroborates this interpretation since the overall PL emission increases with the density of ion-induced radiation damage in the host crystal.[24]

As stated earlier, the anti-bunching of emission from individual spots was verified by HBT interferometry on a set of ∼10 emitters for each of the considered regions following each processing step. The characterization of two exemplary emitters, associated with ZPLs at ∼560 nm [corresponding to the emission spot circled in white and labeled as "C1," in Fig. 2(k)] and ∼600 nm [labeled "C2" in Fig. 2(i)] is shown in Figs. 6 and 7, respectively. The second-order autocorrelation histogram acquired via HBT interferometry at different optical excitation powers [Fig. 6(a) and 7(a)] highlighted the occurrence

of non-classical emission originating from an individual source in both cases [i.e., $g^2(t=0) < 0.5$]. The curves were fitted according to a model based on a three-level system that allows for the presence of a metastable shelving state,[2]

$$g^{(2)}(t) = 1 - (1 + a) \cdot \exp(-|t| \cdot \lambda_1) + a \cdot \exp(-|t| \cdot \lambda_2) + b. \quad (1)$$

Under vanishing optical excitation power, the decay rate through the shelving state of the three level system is negligible with respect to that of the radiative transition. The excited state lifetime was estimated as (3.4 ± 0.2) ns for the C1 center and (5.7 ± 0.5) ns for the C2 center by a linear regression of the λ_1 parameter vs the optical excitation power [Figs. 6(b) and 7(b), respectively]. The emission intensity and excitation power at saturation parameters were determined to be (119 ± 9) kcps and (0.28 ± 0.09) mW for the C1 center [Fig. 6(c)] and 65 ± 8 kcps and (0.16 ± 0.06) mW for the C2 center [Fig. 7(c)]. In addition to the aforementioned ZPL, the spectral signature of both emitters [Figs. 6(d) and 7(d)] within the passband 550–650 nm used for our filtering optics consisted of broad spectra. It is also worth mentioning that the emission intensity in saturation conditions refers only to the aforementioned spectral range, and that the overall emission intensity of the emitters is higher. The observed differences in the centers lifetime, emission intensity, and excitation power in saturation conditions could be explained by considering the different spectral signatures of the centers as indicative of different defective complexes, both being compatible with what was previously reported in the scientific literature for unimplanted AlN.[38]

Finally, additional insight in the role of the thermal annealing was obtained by performing an analysis on the C2 emitter located in the unimplanted region, following each thermal treatment (Fig. 8).
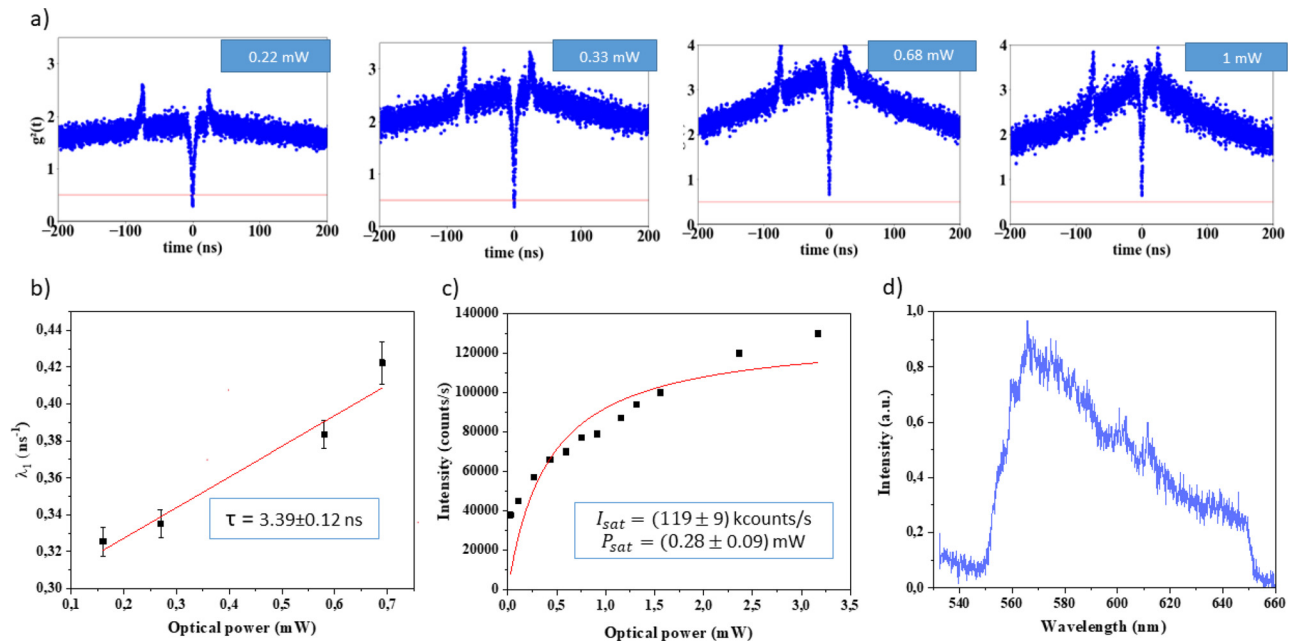
FIG. 6. Anti-bunched emission parameters from an individual center in the region implanted at 10^{13} cm^{-2} fluence after the 600 °C thermal processing. The emitter is circled in white and labeled as "C1" in Fig. 2(k). (a) Second-order correlation measurements and lifetime extracted from the power dependence of the λ_1 fitting parameter. The peaks at $t \sim -2$ ns and $t \sim +80$ ns correspond to the backflash peaks of the detection system, originating from photon backflash from one single-photon detector reaching the other detector through the reflection of photons at the terminations of the two branches of the fiber-coupled HBT interferometer. (b) Linear regression of the λ_1 parameter as a function of the excitation power. (c) Saturation curve of the emitter, after background subtraction. (d) PL spectrum with spectral filtering to remove light outside the 550–650 nm range.

FIG. 7. Anti-bunched emission parameters from an individual center in the unimplanted region after the 400 °C thermal processing. The emitter is circled in white and labeled as "C2" in Fig. 2(i). (a) Second-order correlation measurements and lifetime extracted from the power dependence of the λ_1 fitting parameter. (b) Linear regression of the λ_1 parameter as a function of the excitation power. (c) Saturation curve of the emitter, after background subtraction. (d) PL spectrum with spectral filtering to remove light outside the 550–650 nm range.
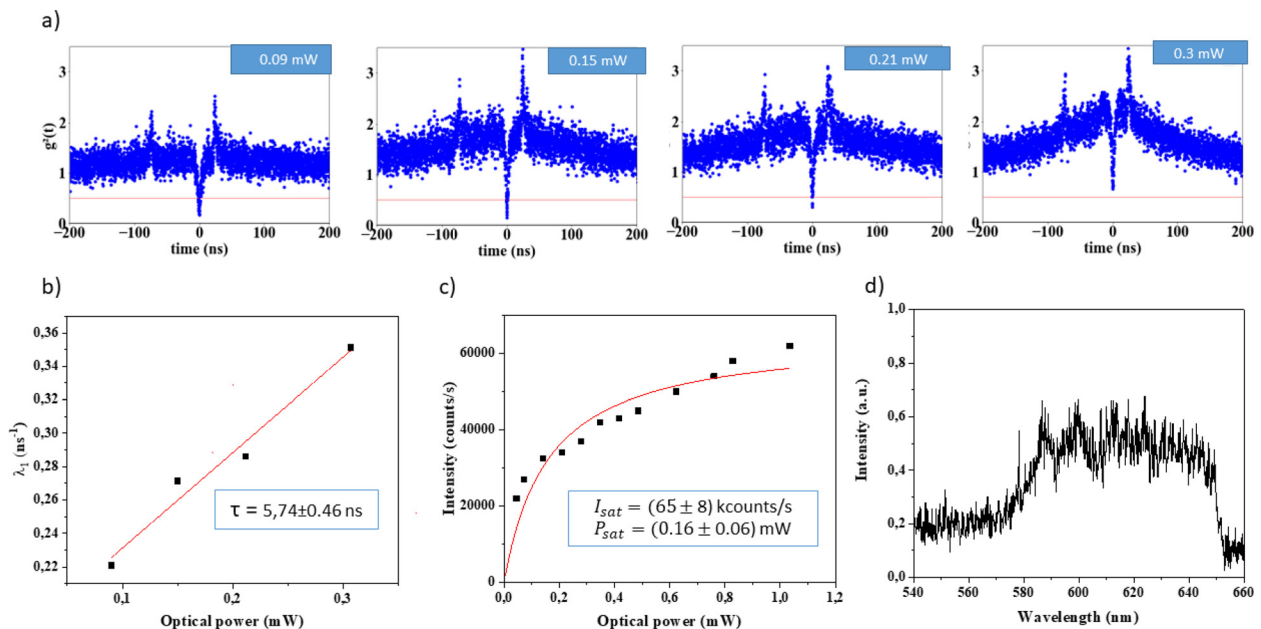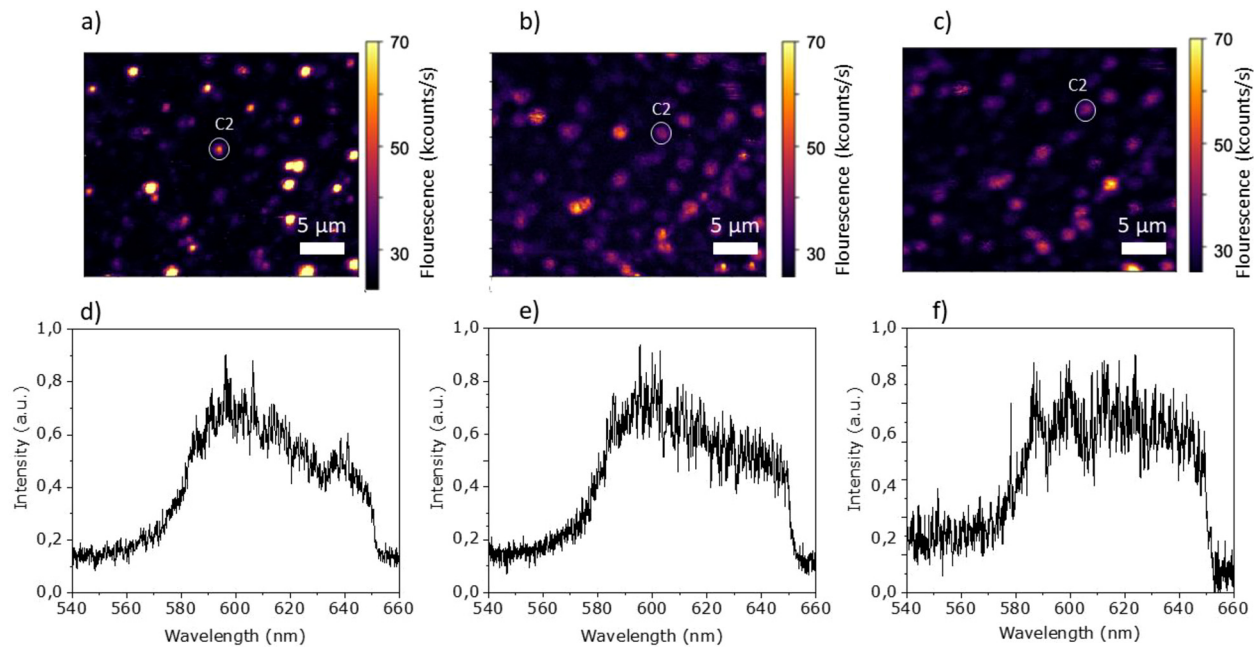
FIG. 8. Spectral comparison of the same single emitter (labeled as "C2" in the PL maps isolated in the unimplanted region after each post-implantation process): (a) pristine material; (b) following 400 °C thermal annealing; and (c) following 600 °C thermal annealing.

The center exhibited a broad emission band centered at ~600 nm, which was left unchanged by the subsequent annealing steps. This observation indicates that the isolated defect was still optically active after annealing at temperatures as high as 600 °C and that its emission spectrum was not altered by the thermal process.

To summarize, in this paper, we performed a systematic investigation on the role of ion implantation in the formation of single-photon emitting intrinsic defects in AlN. We demonstrated that the implantation of 60 keV Al⁻ ions increases the density of individual color centers, and the background emission intensity was correlated with the ion fluence. The study of which of these optically active quantum emitters corresponded to an already present center and which to an implanted one was out of the scope of this work but would require a specific investigation to analyze the properties of the implanted defects. The highest formation yield was achieved upon irradiation at 1×10^{13} cm^{-2} fluence, without any subsequent thermal treatment of the sample. Higher ion fluences resulted in the formation of emitter ensembles that resulted in a limited capability to isolate single color centers. A spectral analysis of the emitters revealed that all the point defects analyzed in the ion implantation region have similar features with respect to those found in pristine AlN, thus highlighting that Al⁻ ion implantation results in the formation of intrinsic defects, in other words that the emitters are not related to the introduction of foreign chemical species in the AlN lattice. The structural and spectral stability of individual color centers following thermal processes up to 600 °C was also demonstrated. These results show a viable pathway, based on industry-compatible ion implantation technique that in perspective can be potentially scaled to the single-ion delivery level,[9,11] for the fabrication of quantum emitters in chip-integrable AlN platform.

AUTHOR DECLARATIONS
Conflict of Interest

The authors have no conflicts to disclose.

Author Contributions

E. Nieto Hernández: Conceptualization (equal); Formal analysis (equal); Investigation (equal); Methodology (equal); Writing – original draft (equal). **H. B. Yağcı:** Methodology (equal); Writing – review & editing (equal). **V. Pugliese:** Investigation (equal); Writing – review & editing (equal). **P. Aprà:** Resources (equal); Writing – review & editing (equal). **J. K. Cannon:** Writing – review & editing (equal). **S. G. Bishop:** Writing – review & editing (equal). **J. Hadden:** Conceptualization (equal); Funding acquisition (equal); Project administration (equal); Supervision (equal); Writing – review & editing (equal). **S. Ditalia Tchernij:** Methodology (equal); Writing – review & editing (equal). **P. Olivero:** Funding acquisition (equal); Project administration (equal); Supervision (equal); Writing – review & editing (equal). **A. J. Bennett:** Conceptualization (equal); Funding acquisition (equal); Project administration (equal); Supervision (equal); Writing – review & editing (equal). **J. Forneris:** Conceptualization (equal); Funding acquisition (equal); Project administration (equal); Supervision (equal); Writing – original draft (equal).

DATA AVAILABILITY

The data that support the findings of this study are available from the corresponding author upon reasonable request.

REFERENCES

[1]D. D. Awschalom, R. Hanson, J. Wrachtrup et al., "Quantum technologies with optically interfaced solid-state spins," Nat. Photonics **12**, 516 (2018).

[2]C. Bradac, W. Gao, J. Forneris et al., "Quantum nanophotonics with group IV defects in diamond," Nat. Commun. **10**, 5625 (2019).

[3]P. Rembold, N. Oshnik, M. M. Muller et al., "Introduction to quantum optimal control for quantum sensing with nitrogen-vacancy centers in diamond," AVS Quantum Sci. **2**, 024701 (2020).

[4]P. Michler, A. Kiraz, C. Becher et al., "A quantum dot single-photon turnstile device," Science **290**, 2282 (2000).

[5]C. Kurtsiefer, S. Mayer, P. Zarda et al., "Stable solid-state source of single photons," Phys. Rev. Lett. **85**, 290 (2000).

[6]M. Radulaski, M. Widmann, M. Niethammer et al., "Scalable quantum photonics with single color centers in silicon carbide," Nano Lett. **17**, 1782 (2017).

[7]S. A. Momenzadeh, R. J. Stohr, F. Favaro de Oliveira et al., "Nanoengineered diamond waveguide as a robust bright platform for nanomagnetometry using shallow nitrogen vacancy centers," Nano Lett. **15**, 165 (2015).

[8]X.-J. Wang, H.-H. Fang, F.-W. Sun, and H.-B. Sun, Laser & Photonics Rev. **16**, 2100029 (2022).

[9]M. Lesik, P. Spinicelli, S. Pezzagna et al., "Maskless and targeted creation of arrays of colour centres in diamond using focused ion beam technology," Phys. Status Solidi A **210**, 2055 (2013).

[10]T. Lühmann, R. John, R. Wunderlich et al., "Coulomb-driven single defect engineering for scalable qubits and spin sensors in diamond," Nat. Commun. **10**, 4956 (2019).

[11]J. L. Pacheco, M. Singh, D. L. Perry et al., "Ion implantation for deterministic single atom devices," Rev. Sci. Instrum. **88**, 123301 (2017).

[12]Y. Zhou, Z. Mu, G. Adamo et al., "Direct writing of single germanium vacancy center arrays in diamond," New J. Phys. **20**, 125004 (2018).

[13]L. Hussey, I. Bryan, R. Kirste et al., "Direct observation of the polarity control mechanism in aluminum nitride grown on sapphire by aberration corrected scanning transmission electron microscopy," Microsc. Microanal. **20**, 162 (2014).

[14]R. Boichot, A. Claudel, N. Baccar et al., "Epitaxial and polycrystalline growth of AlN by high temperature CVD: Experimental results and simulation," Surf. Coat. Technol. **205**, 1294 (2010).

[15]D. Alden, W. Guo, R. Kirste et al., "Fabrication and structural properties of AlN submicron periodic lateral polar structures and waveguides for UV-C applications," Appl. Phys. Lett. **108**, 261106 (2016).

[16]J. Wang, Y. Zhou, Z. Wang et al., "Bright room temperature single photon source at telecom range in cubic silicon carbide," Nat. Commun. **9**, 4106 (2018).

[17]Y. Zhou, Z. Wang, A. Rasmita et al., "Room temperature solid-state quantum emitters in the telecom range," Sci. Adv. **4**, eaar3580 (2018).

[18]A. Senichev, Z. O. Martin, S. Peana et al., "Room-temperature single-photon emitters in silicon nitride," Sci. Adv. **7**, eabj0627 (2021).

[19]G. Zhang, Y. Cheng, J.-P. Chou et al., "Material platforms for defect qubits and single-photon emitters," Appl. Phys. Rev. **7**, 031308 (2020).

[20]C. Wang, C. Kurtsiefer, H. Weinfurter et al., "Single photon emission from SiV centres in diamond produced by ion implantation," J. Phys. B: At. Mol. Opt. Phys. **39**, 37 (2006).

[21]T. Iwasaki, F. Ishibashi, Y. Miyamoto et al., "Germanium-vacancy single color centers in diamond," Sci. Rep. **5**, 12882 (2015).

[22]I. Aharonovich, S. Castelletto, B. C. Johnson et al., "Chromium single-photon emitters in diamond fabricated by ion implantation," Phys. Rev. B **81**, 121201 (2010).

[23]T. Gaebel, I. Popa, A. Gruber et al., "Stable single-photon source in the near infrared," New J. Phys. **6**, 98 (2004).

[24]S. D. Tchernij, T. Herzig, J. Forneris et al., "Single-photon-emitting optical centers in diamond fabricated upon Sn implantation," ACS Photonics **4**, 2580 (2017).

[25]M. Widmann, S.-Y. Lee, T. Rendler et al., "Coherent control of single spins in silicon carbide at room temperature," Nat. Mater. **14**, 164 (2015).

[26]S. Castelletto, B. C. Johnson, V. Ivady et al., "A silicon carbide room-temperature single-photon source," Nat. Mater. **13**, 151 (2014).

[27]M. Hollenbach, Y. Berencen, U. Kentsch et al., "Engineering telecom single-photon emitters in silicon for scalable quantum photonics," Opt. Express **28**, 26111 (2020).

[28]A. Durand, Y. Baron, W. Redjem et al., "Broad diversity of near-infrared single-photon emitters in silicon," Phys. Rev. Lett. **126**, 083602 (2021).

[29]Y. Baron, A. Durand, P. Udvarhelyi et al., "Detection of single W-centers in silicon," ACS Photonics **9**, 2337 (2022).

[30]Y. Xue, F. Chen, Z. Fang et al., "Bright room temperature near-infrared single-photon emission from single point defects in the AlGaN film," Appl. Phys. Lett. **118**, 131103 (2021).

[31]A. M. Berhane, K.-Y. Jeong, Z. Bodrog et al., "Bright room-temperature single-photon emission from defects in gallium nitride," Adv. Mater. **29**, 1605092 (2017).

[32]G. Grosso, H. Moon, B. Lienhard et al., "Tunable and high-purity room temperature single-photon emission from atomic defects in hexagonal boron nitride," Nat. Commun. **8**, 705 (2017).

[33]N. V. Proscia, Z. Shotan, H. Jayakumar et al., "Near-deterministic activation of room-temperature quantum emitters in hexagonal boron nitride," Optica **5**, 1128 (2018).

[34]P. Khatri, A. J. Ramsay, R. N. E. Malein et al., "Optical gating of photoluminescence from color centers in hexagonal boron nitride," Nano Lett. **20**, 4256 (2020).

[35]T.-J. Lu, B. Lienhard, K.-Y. Jeong et al., "Bright high-purity quantum emitters in aluminum nitride integrated photonics," ACS Photonics **7**, 2650 (2020).

[36]Y. Xue, H. Wang, N. Xie et al., "Single-photon emission from point defects in aluminum nitride films," J. Phys. Chem. Lett. **11**, 2689 (2020).

[37]S. G. Bishop, J. P. Hadden, F. D. Alzahrani et al., "Room-temperature quantum emitter in aluminum nitride," ACS Photonics **7**, 1636 (2020).

[38]C. Xiong, W. H. P. Pernice, X. Sun et al., "Aluminum nitride as a new material for chip-scale optomechanics and nonlinear optics," New J. Phys. **14**, 095014 (2012).

[39]J. R. Weber, W. F. Koehl, J. B. Varley et al., "Quantum computing with defects," Proc. Natl. Acad. Sci. U. S. A. **107**, 8513 (2010).

[40]Y. Tu, Z. Tang, G. Zhao et al., "A paramagnetic neutral VAlON center in wurtzite AlN for spin qubit application," Appl. Phys. Lett. **103**, 072103 (2013).

[41]H. Seo, M. Govoni, and G. Galli, "Design of defect spins in piezoelectric aluminum nitride for solid-state hybrid quantum technologies," Sci. Rep. **6**, 20803 (2016).

[42]X.-J. Wang, S. Zhao, H.-H. Fang *et al.*, "Quantum emitters with narrow band and high Debye–Waller factor in aluminum nitride written by femtosecond laser," Nano Lett. **23**, 2743 (2023).

[43]J. F. Ziegler, "SRIM-2003," Nucl. Instrum. Methods Phys. Res., Sect. B **219–220**, 1027 (2004).

[44]Q. Ma and D. R. Clarke, "Optical fluorescence from chromium ions in sapphire: A probe of the image stress," Acta Metall. Mater. **41**, 1811 (1993).

[45]J. M. Binder, A. Stark, N. Tomek *et al.*, "Qudi: A modular python suite for experiment control and data processing," SoftwareX **6**, 85 (2017).

[46]E. Corte, G. Andrini, E. N. Hernandez *et al.*, "Magnesium-vacancy optical centers in diamond," ACS Photonics **10**, 101 (2023).

05 April 2024 11:42:11